Ordered Hierarchical Nanostructured Carbon as a Highly Efficient Cathode Catalyst Support in Proton Exchange Membrane Fuel Cell

Baizeng Fang, Jung Ho Kim, Minsik Kim, and Jong-Sung Yu*

Department of Advanced Materials Chemistry, Korea University, 208 Seochang, Jochiwon, ChungNam 339-700, Republic of Korea

Received May 30, 2008. Revised Manuscript Received November 21, 2008

Ordered hierarchical nanostructured carbon (OHNC) has been fabricated through inverse replication of silica template and explored for the first time to support high loading of Pt nanoparticles as cathode catalyst in proton exchange membrane fuel cells (PEMFC). The superb characteristics such as ordered hierarchical nanostructure, large surface area, and mesopore volume enable the OHNC to support high loading (60 wt %) of Pt nanoparticles with uniform dispersion and small particle size. Compared to carbon black Vulcan XC-72 (VC)-supported Pt (60 wt %), the OHNC-supported one has exhibited greatly enhanced catalytic activity toward oxygen reduction reaction by ca. 53−88% and considerably improved PEMFC performance. More importantly, unlike the VC-supported Pt catalysts, the OHNC-supported Pt (40 or 60 wt %) outperforms the OHNC-supported Pt (20 wt %) even at a low catalyst loading of 0.2 mg Pt/cm^2 in the cathode, which represents a significant breakthrough in fuel cell technology because of the expectable marked reduction in fabricating cost of the supported Pt catalyst and the corresponding system weight and considerably improved fuel cell performance.

1. Introduction

Ordered porous carbon materials with three-dimensionally interconnected pore structures and highly developed porosity have a variety of potential applications such as catalyst supports in low temperature fuel cells,[1,2] electrode materials for electric double-layer capacitors[3,4] and for lithium ion batteries,[5] adsorbents, and hydrogen storage materials.[6−11] Recently, much attention has been paid to fabrication of porous carbon materials with hierarchical porosity due to their unique structural characteristics, namely, macropores in combination with micropores or mesopores,[12−15] which allow not only enhanced selective access to the micropores (or smaller mesopores) but also efficient mass transport through the macropores (or larger mesopores). However, the pores in these hierarchical carbon materials are randomly and disorderly distributed. In our recent paper, highly ordered porous carbon material with hierarchical nanostructure has been developed and promising application in direct methanol fuel cell (DMFC) demonstrated.[16]

Proton exchange membrane fuel cells (PEMFCs) have been of great interest as future energy sources for applications such as low/zero-emission electric vehicles, distributed home power generators, and power sources for small portable electronics because of their high power density, relatively quick startup, rapid response to varying loading, and relatively low operating temperature.[17−22] In particular, hydrogen-fueled PEMFCs produce no pollutants such as NO_x, SO_x, or CO_2 and are thereby considered to be environmentally benign. However, the commercial viability of the PEMFCs technology has been hindered by several challenges, including poor kinetics of the oxygen reduction reaction (ORR) and the high cost of noble metal (i.e., Pt) catalysts. One effective approach to decrease the cost of

* To whom correspondence should be addressed. E-mail: jsyu212@korea.ac.kr.

(1) (a) Liu, H.; Song, C.; Zhang, L.; Zhang, J.; Wang, H.; Wilkinson, D. P. *J. Power Sources* **2006**, *155*, 95–110. (b) Joo, S.-H.; Choi, S.-J.; Oh, I.; Kwak, J.; Liu, Z.; Terasaki, O.; Ryoo, R. *Nature* **2001**, *412*, 169–172.
(2) Yu, J.-S.; Kang, S.; Yoon, S. B.; Chai, G. S. *J. Am. Chem. Soc.* **2002**, *124*, 9382–9383.
(3) Lee, J.; Yoon, S.; Oh, S.-M.; Shin, C.-H.; Hyeon, T. *Adv. Mater.* **2000**, *12*, 359–362.
(4) Zhou, H.-S.; Zhu, S.; Hibino, M.; Honma, I. *J. Power Sources* **2003**, *122*, 219–223.
(5) Zhou, H.-S.; Zhu, S.; Hibino, M.; Honma, I.; Ichihara, M. *Adv. Mater.* **2003**, *15*, 2107–2111.
(6) Fang, B.; Kim, M.; Kim, J. H.; Yu, J. S. *Langmuir* **2008**, *24*, 12068–12072.
(7) Marsh, H. *Introduction to Carbon Science*; Butterworths: London, 1989.
(8) Patrick, J.-W. *Porosity in Carbons: Characterization and Applications*; Edward Arnold: London, 1995.
(9) Frackowiak, E.; Béguin, F. *Carbon* **2001**, *39*, 937–950.
(10) Lillo-Rodenas, M. A.; Lozano-Castello, D.; Cazorla-Amoros, D.; Linares-Solano, A. *Carbon* **2001**, *39*, 751–759.
(11) Fang, B.-Z.; Zhou, H.-S.; Honma, I. *J. Phys. Chem. B* **2006**, *110*, 4875–4880.
(12) Yoon, S. B.; Sohn, K.; Kim, J.-Y.; Shin, C.-H.; Yu, J.-S.; Hyeon, T. *Adv. Mater.* **2002**, *14*, 19–21.
(13) Ren, J.; Ding, J.; Chan, K.-Y.; Wang, H. *Chem. Mater.* **2007**, *19*, 2786–2795.
(14) Taguchi, A.; Smatt, J.-H.; Linden, M. *Adv. Mater.* **2003**, *15*, 1209–1211.
(15) Yuan, Z.-Y.; Su, B.-L. *J. Mater. Chem.* **2006**, *16*, 663–677.
(16) Chai, G. S.; Shin, I. S.; Yu, J.-S. *Adv. Mater.* **2004**, *16*, 2057–2061.
(17) Oliveira, N. A.; Franco, E. G.; Arico, E.; Linardi, M.; Gonzalez, E. R. *J. Eur. Ceram. Soc.* **2003**, *23*, 2987–2992.
(18) Toda, T.; Igarashi, H.; Uchida, H.; Watanabe, M. *J. Electrochem. Soc.* **1999**, *146*, 3750–3756.
(19) Springer, T. E.; Zawodzinski, T. A.; Gottesfeld, S. *J. Electrochem. Soc.* **1991**, *138*, 2334–2342.
(20) Service, R. *Science* **2002**, *296*, 1222–1224.
(21) Huang, Y.; Wang, A.; Li, L.; Wang, X.; Su, D.; Zhang, T. *J. Catal.* **2008**, *255*, 144–152.
(22) Matter, P. H.; Zhang, L.; Ozkan, U. S. *J. Catal.* **2006**, *239*, 83–96.

10.1021/cm801467y CCC: $40.75
Published on Web 02/04/2009

catalysts is alloying of Pt with transition metals such as Fe, Co, Ni, Sn,[23−29] Bi, In, Pb, and Cu,[30,31] with less expensive noble metals such as Ir,[32,33] Ru,[34−37] Rh,[37−39] and Au,[40] or using non-Pt metal such as Pd[41] or Pd-based alloys such as Pd−Co,[42] Pd−Co−Au,[43] or WC.[44]

Catalyst support technology has been proved as another effective approach to lower the usage of noble metal in catalysts and meanwhile to improve the catalytic activity of the supported catalysts. It has been recognized that the catalytic activity of the Pt based catalysts is strongly dependent on catalyst supports,[45−>51] which are highly needed to distribute and stabilize the catalyst particles in the catalytic system. In addition, the supports play a very important role in determining the size, dispersion degrees,[52−55] and alloyed degree[56] of catalysts and diffusion kinetics of reactants and products[45−51] and hence contribute a lot to the catalytic activity of the supported catalysts. Synthesis of Pt nanoparticles as electrocatalytic materials with uniform size and good dispersion on their support has thus become of paramount importance. Carbon black Vulcan XC-72 (VC) is widely used as an electrocatalyst support in the PEMFCs due to its relatively large surface area and excellent chemical stability in the fuel cell environment.[52−55] However, the carbon black VC contains approximately 47% of micropores,[57,58] some of which are too small (less than 1 nm in diameter) to be accessible to the electrolyte polymer, resulting in entrapped Pt nanoparticles, which do not contribute to the electrode reactions due to the absence of the triple-phase boundaries (i.e., gas−electrolyte−electrode).

Some novel nanostructured carbon materials have been investigated as possible catalyst supports for hydrogen-fueled PEMFCs recently, including carbon nanotubes (CNTs)[59−67] and carbon nanofibers (CNFs).[68] Although the CNT-supported Pt electrode showed approximately 20% higher power density than the VC-supported one,[66] realistic application of CNTs has been hindered by several difficulties associated with their processes involving synthesis, purification, dispersion, and surface activation. Presently, high quality CNTs are still produced on a very small scale, and the process is extremely costly.[69] CNF-supported Pt (20 wt %) only exhibited a slightly improved electrocatalytic performance than the VC supported one.[68]

(23) Stamenkovic, V.; Grgur, B. N.; Ross, P. N.; Markovic, N. M. *J. Electrochem. Soc.* **2005**, *152*, A277−A282.
(24) Salgado, J. R. C.; Antolini, E.; Gonzalez, E. R. *J. Phys. Chem. B* **2004**, *108*, 17767–17774.
(25) Yu, P.; Pemberton, M.; Plasse, P. *J. Power Sources* **2005**, *144*, 11–20.
(26) Xiong, L.; Manthiram, A. *J. Mater. Chem.* **2004**, *14*, 1454–1460.
(27) Paulus, U. A.; Wokaun, A.; Scherer, G. G.; Schmidt, T. J.; Stamenkovic, V.; Radmilovic, V.; Markovic, N. M.; Ross, P. N. *J. Phys. Chem. B* **2002**, *106*, 4181–4191.
(28) Ioroi, T.; Yasuda, K. *J. Electrochem. Soc.* **2005**, *152*, A1917−A1924.
(29) Brandon, N. P.; Skinner, S.; Steele, B. C. H. *Annu. Rev. Mater. Res.* **2003**, *33*, 183–213.
(30) Casado-Rivera, E.; Volpe, D. J.; Alden, L.; Lind, C.; Downie, C.; Vazquez-Alvarez, T.; Angelo, A. C. D.; DiSalvo, F. J.; Abruna, H. D *J. Am. Chem. Soc.* **2004**, *126*, 4043–4049.
(31) Marković, N. M.; Schmidt, T. J.; Stamenković, V.; Ross, P. N. *Fuel Cells* **2001**, *1*, 105–116.
(32) Chen, G.-Y.; Delafuente, D. A.; Sarangapani, S.; Mallouk, T. E. *Catal. Today* **2001**, *67*, 341–355.
(33) Liao, S.-J.; Holmes, K.-A.; Tsaprailis, H.; Birss, V. I. *J. Am. Chem. Soc.* **2006**, *128*, 3504–3505.
(34) Waszczuk, P.; Solla-Gullön, J.; Kim, H.-S.; Tong, Y. Y.; Montiel, V.; Aldaz, A.; Wieckowski, A. *J. Catal.* **2001**, *203*, 1–6.
(35) Huang, S.; Chang, C.; Yeh, C. *J. Catal.* **2006**, *241*, 400–406.
(36) (a) Sivakumar, P.; Tricoli, V. *Electrochim. Acta* **2006**, *51*, 1235–1243. (b) Sivakumar, P.; Tricoli, V. *Electrochem. Solid-State Lett.* **2006**, *9*, A167−A170.
(37) (a) Park, K. W.; Ahn, K. S.; Choi, J. H.; Nah, Y. C.; Sung, Y. E. *Appl. Phys. Lett.* **2003**, *82*, 1090–1092. (b) Park, K.-W.; Choi, J.-H.; Lee, S.-A.; Pak, C. H.; Chang, H.; Sung, Y. E. *J. Catal.* **2004**, *224*, 236–242.
(38) Strohm, J.; Zheng, J.; Song, C. *J. Catal.* **2006**, *238*, 309–320.
(39) Kugai, J.; Subramani, V.; Song, C.; Engelhard, M. H.; Chin, Y. *J. Catal.* **2006**, *238*, 430–440.
(40) (a) Zhou, S.; Jackson, G. S.; Eichhorn, B. *Adv. Funct. Mater.* **2007**, *17*, 3099–3104. (b) Luo, J.; Njoki, P. N.; Lin, Y.; Wang, L.-Y.; Zhong, C.-J. *Electrochem. Commum.* **2006**, *8*, 581–587.
(41) Papageorgopoulos, D. C.; Keijzer, M.; Veldhuis, J. B. J.; A.; Bruijn, F. de. *J. Electrochem. Soc.* **2002**, *149*, A1400−A1404.
(42) Fernandez, J. L.; Walsh, D. A.; Bard, A. J. *J. Am. Chem. Soc.* **2005**, *127*, 357–365.
(43) Raghuveer, V.; Ferreira, P. J.; Manthiram, A. *Electrochem. Commun.* **2006**, *8*, 807–814.
(44) Yang, X. G.; Wang, C. Y. *Appl. Phys. Lett.* **2005**, *86*, 224104-1–224104-3.
(45) (a) Shanmugam, S.; Gedanken, A. *Small* **2007**, *3*, 1189–1193. (b) Chai, G. S.; Yoon, S. B.; Yu, J.-S.; Choi, J.-H.; Sung, Y.-E. *J. Phys. Chem. B* **2004**, *108*, 7074–7079.
(46) (a) Fang, B.; Kim, J. H.; Yu, J.-S. *Elecrochem. Commun.* **2008**, *10*, 659–662. (b) Fang, B.; Kim, J. H.; Lee, C.; Yu, J.-S. *J. Phys. Chem. C* **2008**, *112*, 639–645. (c) Fang, B.; Kim, M.; Lee, C.; Yu, J.-S. *Appl. Catal. B: Environ.* **2008**, *84*, 100–105.
(47) (a) Chai, G. S.; Yoon, S. B.; Kim, J. H.; Yu, J.-S. *Chem. Commun.* **2004**, *23*, 2766–2767. (b) Chai, G. S.; Yoon, S. B.; Yu, J.-S. *Carbon* **2005**, *43*, 3028–3031. (c) Kim, M.; Hwang, S.; Yu, J. -S. *J. Mater. Chem.* **2007**, *17*, 1656–1659.
(48) Raghuveer, V.; Manthiram, A. *J. Electrochem. Soc.* **2005**, *152*, A1504−A1508.
(49) Rao, V.; Simonov, P. A.; Savinova, E. R.; Plaksin, G.; Cherepanova, S.; Kryukova, G.; Stimming, U. *J. Power Sources* **2005**, *145*, 178–187.
(50) (a) Chan, K.-Y.; Ding, J.; Ren, J.; Cheng, S.; Tsang, K. Y. *J. Mater. Chem.* **2004**, *14*, 505–516. (b) Chang, H.; Joo, S. H.; Pak, C. *J. Mater. Chem.* **2007**, *17*, 3078–3088.
(51) (a) Tian, Z. Q.; Jiang, S. P.; Liang, Y. M.; Shen, P. K *J. Phys. Chem. B* **2006**, *110*, 5343–5350. (b) Su, F.; Zhao, X. S.; Wang, Y.; Zeng, J.; Zhou, Z.; Lee, J. Y. *J. Phys. Chem. B* **2005**, *109*, 20200–20206.
(52) Arico, A. S.; Pino, L.; Antonucci, P. L.; Giordano, N. *Carbon* **1990**, *28*, 599–609.
(53) Kinoshita, K. *Electrochemical Oxygen Technology*; John Wiley & Sons: New York, 1992.
(54) Qu, Z.; Huang, W.; Zhou, S.; Zheng, H.; Liu, X.; Cheng, M.; Bao, X. *J. Catal.* **2005**, *234*, 33–36.
(55) Prado-Burguette, C.; Linares-Solano, A.; Rodiguez-Reinoso, F.; Salinas-Martinez de Lecea, C. *J. Catal.* **1989**, *115*, 98–106.
(56) Takasu, Y.; Kawaguchi, T.; Sugimoto, W.; Murakami, Y. *Electrochim. Acta* **2003**, *48*, 3861–3868.
(57) Park, P. W.; Kwon, B. K.; Choi, J. H.; Park, I. S.; Kim, Y. M.; Sung, Y. E. *J. Power Sources* **2002**, *109*, 439–445.
(58) Uchida, M.; Aoyama, Y.; Tanabe, M.; Yanagihara, N.; Eda, N.; Ohta, A. *J. Electrochem. Soc.* **1995**, *142*, 2572–2576.
(59) Lee, K.; Zhang, J.; Wang, H.; Wilkinson, D. P. *J. Appl. Electrochem.* **2006**, *36*, 507–522.
(60) Wang, C.; M.; Waje,; Wang, X.; Tang, J. M.; Haddon, R. C.; Yan, Y. *Nano Lett.* **2004**, *4*, 345–348.
(61) Liu, Z.; Lin, X.; Lee, J.-Y.; Zhang, W.-S.; Han, M.; Gan, L.-M. *Langmuir* **2002**, *18*, 4054–4060.
(62) Li, X.; Hsing, I.-M. *Electrochim. Acta* **2006**, *51*, 5250–5258.
(63) Li, W.; Wang, X.; Chen, Z.; Waje, M.; Yan, Y. *Langmuir* **2005**, *21*, 9386–9389.
(64) Gangeri, M.; Centi, G.; Malfa, A. La; Perathoner, S.; Vieira, R.; Pham-Huu, C.; Ledoux, M. J. *Catal. Today* **2005**, *102*, 50–57.
(65) Matsumoto, T.; Komatsu, T.; Arai, K.; Yamazaki, T.; Kijima, M.; Shimizu, H.; Takasawa, Y.; Nakamura, J. *Chem. Commun.* **2004**, *7*, 840–841.
(66) Girishkumar, G.; Retter, M.; Underhile, R.; Binz, D.; Vinodgopal, K.; McGinn, P.; Kamat, P. *Langmuir* **2005**, *21*, 8487–8494.
(67) Wildgoose, G. G.; Banks, C. E.; Compton, R. G. *Small* **2006**, *2*, 182–193.
(68) Yuan, F. L.; Ryu, H. *Nanotechnology* **2004**, *15*, s596−s602.
(69) Baughman, R. H.; Zakhidov, A. A.; De Heer, W. A. *Science* **2002**, *297*, 787–792.

In our previous study, a novel ordered hierarchical nanostructured carbon (OHNC), namely, periodically ordered bimodal porous carbon (POBPC), had been developed and explored as an anode catalyst support in DMFC.[16] Although the POPBC-supported Pt−Ru catalyst has demonstrated good catalytic activity toward methanol oxidation, whether the POPBC is an ideal cathode catalyst support for ORR in hydrogen-fueled PEMFC still remains a question because the working environment in the cathode compartment of PEMFC is considerably different from that in the anode compartment of DMFC. For the supported cathode catalyst more tolerance of the aggressive oxidative environment is required in addition to a high catalytic activity toward sluggish ORR while for the anode catalyst more attention has to be paid to the tolerance of the impurity in the fuel and intermediate of the oxidation reaction (such as CO). This is why many of the research efforts have been made to develop specific and different anode and cathode catalyst metals and/or support materials tailored for their specific working conditions. Recently, Ding et al. reported a very noteworthy and interesting result that the Pt supported on the ordered mesoporous carbon CMK-3 outperformed a commercial Pt/C electrocatalyst for ORR on a gas-diffusion electrode while the Pt−Ru supported on the same support of CMK-3 was not as effective for methanol oxidation.[70] Although they claimed the inferiority in catalytic activity toward methanol oxidation of the CMK-3-supported Pt−Ru was in part attributable to its slightly less Pt−Ru loading than the commercial one, they had to admit the inferiority was also associated to a certain degree with the catalyst support itself. Thus, it seems that there is no universal effective catalyst support suitable for different applications; in other words, an effective anode catalyst support in DMFC may not work well as the cathode catalyst support in PEMFC. In addition, the deposition of platinum nanoparticles at high loading with good dispersion still remains a challenge. In this study, the OHNC has been fabricated through inverse nanocasting of ordered hierarchical nanostructured silica (OHNS) and explored for the first time as a cathode catalyst support in hydrogen-fueled PEMFC. As a result of its fantastic structural characteristics such as large surface area and mesopore volume, enabling the supported Pt nanoparticles to disperse very uniformly with smaller particle size even at a high metal loading of 60 wt %, and ordered macropores in combination with mesopores, providing fast mass transport network around the active sites (locations of Pt nanoparticles), the OHNC-supported Pt (60 wt %) catalysts have demonstrated considerably enhanced catalytic activity toward the ORR and amazing improved PEMFC performance compared to VC-supported ones. It is worthwhile to note that the OHNC-supported high metal loading Pt catalyst (i.e., 60 wt %) outperforms the OHNC-supported low metal loading Pt catalyst (i.e., 20 wt %) even at a low catalyst loading of 0.2 mg Pt/cm^2. This is very significant because the required amount of carbon support will be reduced considerably in the case of Pt (60 wt %)/C compared to Pt (20 wt %)/C, bringing in extra bonus from the supported high metal loading Pt catalyst, namely, low fabrication cost and reduced system weight due to small amount of catalyst support required.

2. Experimental Section

2.1. Synthesis of OHNS and OHNC. OHNS was synthesized using monodisperse polystyrene (PS) spheres as a template with colloidal dispersion of small silica particles as described previously.[16] PS spheres were synthesized using an emulsifier-free polymerization technique described by Dubois et al.[71] A typical synthesis route for the OHNS is as follows: Monodisperse PS spheres were mixed with colloidal dispersion of much smaller silica particles. Upon gradual drying of the mixture, the PS spheres self-assemble themselves into an ordered lattice where the meso-sized smaller silica particles are forced to pack closely at the interstices between the PS spheres, which leads to the generation of particulate silica gels around the ordered PS lattice. Next, the resulting composite was slowly heated to 500 °C and kept for 6 h under air to remove the PS colloids and to sinter the silica nanoparticles, which resulted in OHNS composed of particulate silica gels in the wall of the ordered macropore array. Interestingly, the voids between the sintered silica particles in the resulting OHNS also provide fully interconnected mesopores.

OHNC was synthesized using the OHNS as sacrificial template and furfurylalcohol (FFA) as carbon precursor. The OHNS was dried at 70 °C for 4 h prior to the impregnation with FFA. During the impregnation period, FFA was adsorbed into the mesopore voids between silica particles of the OHNS due to capillary effect. Oxalic acid was added as an acidic catalyst. OHNC was obtained after carbonization of the carbon precursor and subsequent dissolution of the OHNS framework. The removal of the meso-sized silica particles in the OHNS resulted in corresponding mesopores embedded in the carbon wall in addition to the macropores generated by removal of the PS particles. In the present synthesis of carbon, FFA was used as the carbon precursor, and no initiator such as azobisisobutyronitrile (AIBN) was required unlike when divinylbenzene (DVB) was used as the carbon precursor in the previous paper.[16] In addition, compared with DVB, FFA is easier to infiltrate, evenly fill the pores of the silica template, and control the polymerization, and there was no vacuum operation involved in the introduction of the FFA into the silica template, which makes the synthesis of carbon simpler and more feasible compared with the DVB. Furthermore, the OHNC produced by using FFA as the carbon precursor has higher conductivity (as shown in Figure S1 in the Supporting Information) and is more hydrophilic than the carbon produced using DVB as the carbon precursor due to the introduction of hydrophilic surface functional groups (i.e., hydroxyl), resulting in better wetting effect to the catalyst metal precursor (i.e., $H_2PtCl_6 \cdot 6H_2O$) during the impregnation step and accordingly better deposition and dispersion of the supported Pt nanoparticles on the carbon during the subsequent chemical reduction step, and preventing efficiently from agglomeration and particle size growth, which are particularly important and desired for catalyst support material in PEMFC.

2.2. Synthesis of Carbon-Supported Pt Catalysts. Carbon-supported Pt nanoparticle catalysts were prepared by a modified microwave-assisted polyol process described by Liu et al.[72] Typically, 5.0 mL of aqueous solution of 0.05 M $H_2PtCl_6 \cdot 6H_2O$ was mixed with 150 mL of ethylene glycol in a 250 mL beaker. A total of 1.75 mL of 0.4 M KOH was then added dropwise to the

(70) Ding, J.; Chan, K.-Y.; Ren, J.; Xiao, F. *Electrochim. Acta* **2003**, *50*, 3131–3141.

(71) Dubois, E.; Boue, F. *Macromolecules* **2001**, *34*, 3684–3697.

(72) Liu, Z.-L.; Gan, L.-M.; Hong, L.; Chen, W.-X.; Lee, J. Y. *J. Power Sources* **2005**, *139*, 73–78.

vigorously stirred solution to adjust the pH value to around 8−9. Next, the required amount of carbon support was added to the mixture and ultrasonicated for 30 min. The beaker containing the mixture of Pt salt and carbon was heated in a household microwave oven (National NN-S327WF, 2450 MHz, 700 W) for 100 s. The resulting suspension was stirred vigorously overnight and filtered. The residue (mainly carbon-supported Pt catalyst) was washed using deionized water thoroughly and dried at 373 K overnight. Different Pt loadings on the supported catalysts were made, namely, 20, 40, and 60 mass percentage. Actual metal loadings of the supported Pt catalysts were roughly determined by the thermogravimetric analysis (TGA) and found to be very close to the set values.

2.3. Surface Characterization. N_2 adsorption and desorption isotherms were measured at 77 K on a KICT SPA-3000 gas adsorption analyzer after the carbon was degassed at 423 K to 20 μTorr for 12 h. The specific surface areas were determined from nitrogen adsorption using the Brunauer−Emmett−Teller (BET) equation. Total pore volume was determined from the amount of gas adsorbed at the relative pressure of 0.99. Micropore volumes of the porous carbons were calculated from the analysis of the adsorption isotherms using the Horvath−Kawazoe method. Pore size distribution (PSD) was derived from the analysis of the adsorption branch using the Barrett−Joyner−Halenda (BJH) method.

The scanning electron microscopy (SEM) images were obtained using a Hitachi S-4700 microscope operated at an acceleration voltage of 10 kV. High resolution SEM (HRSEM) images were obtained using Hitachi S-5500 microscope operated at 30 kV. The transmission electron microscopy (TEM) was operated on EM 912 Omega at 120 kV. High resolution TEM (HRTEM) images were obtained by using JEOL FE-2010 microscope operated at 200 kV. X-ray diffraction (XRD) measurements for carbon materials and supported Pt catalysts were carried out with a Rigaku 1200 using a Cu Kα radiation and a Ni β-filter operating at 40 kV and 20 mA.

2.4. Preparation of Catalyst Electrodes and Cell Performance Tests. *2.4.1. Half-Cell Test.* For estimation of the electrochemical active surface area of Pt in various carbon-supported Pt catalysts, a three-electrode electrochemical cell (i.e., half-cell) was employed, and cyclic voltammetric (CV) measurements were conducted in 0.5 M H_2SO_4 at room temperature with a scan rate of 25 mV/s. In all cases, Pt gauze was used as the counter electrode and Ag/AgCl as the reference one. Electrolyte solution was deaerated by high-purity nitrogen for 1 h prior to any cyclic voltammetric measurement, and stable voltammograms were recorded after 10 cycles. The working electrode was a thin layer of Nafion-impregnated catalyst cast on a glassy carbon disk (3 mm in diameter) embedded in a Teflon cylinder. The catalyst layer was obtained as follows: First, 5 mg of carbon-supported Pt catalyst was dispersed in 1 mL of solution of deionized water and ethanol (1:4 in volume ratio) and then mixed with 50 μL of Nafion solution (5 wt % Nafion). Next, the mixture was ultrasonicated for 1 h, and a quantity of 5 μL of slurry was pipetted and spread on the top of a glassy carbon disk. Finally, the catalyst-coated glassy carbon electrode was dried at 70 °C for 2 h to yield a loading of 63 μg Pt/cm^2.

2.4.2. Single Cell Test. For evaluation of catalytic activities toward ORR and cell polarization performance of supported Pt catalysts, single cells were constructed. Membrane electrode assembly (MEA) with area of 6.25 cm^2 was employed to construct a single cell, which had been fabricated by hot-pressing a pretreated Nafion 112 (DuPont) sandwiched by the anode and cathode. The Pt loadings were 0.4 mg/cm^2 at the anode and 0.2 mg/cm^2 at the cathode except when stated otherwise. In all cases, Pt (20 wt %)/VC (E-TEK) was used as the anode catalyst. Catalyst inks were prepared by dispersing various carbon-supported Pt nanoparticles into a mixture solution composed of an appropriate amount of deionized water and the required amount of 5 wt % Nafion ionomer solution (Aldrich). The Nafion ionomer contents in the catalyst layers were set as 20 wt % and 25 wt % for the anode and cathode, respectively. The appropriate amount of the catalyst inks was painted uniformly on Teflonized carbon paper (TGPH-090) and dried at 70 °C overnight.

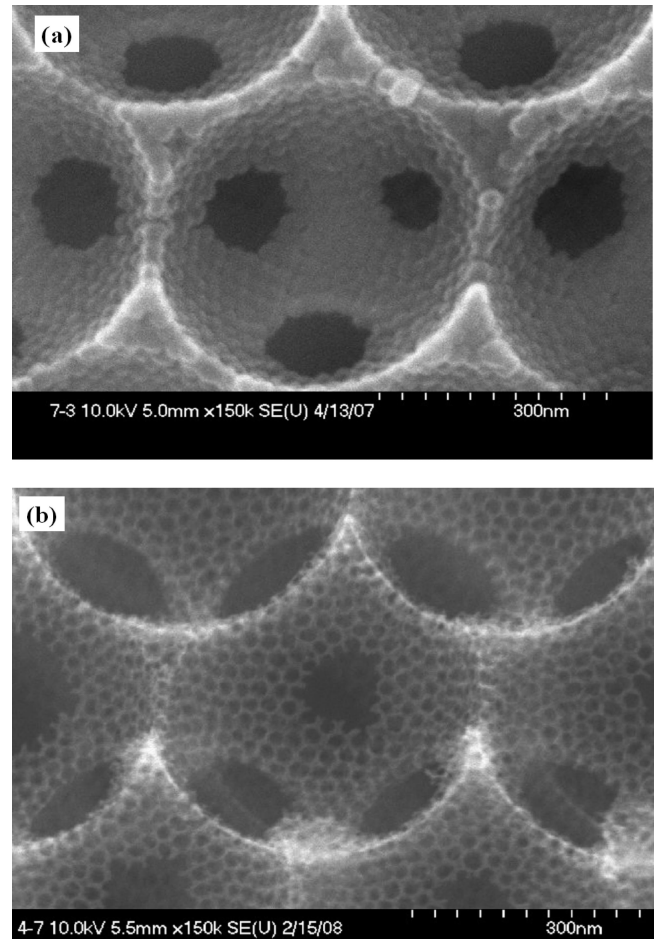

Figure 1. SEM images for the OHNS (a) and the OHNC (b).

Polarization performance tests of supported Pt catalysts were conducted at 60 °C under constant current with a WFCTS fuel cell test station. After being humidified at a temperature of 15 °C higher than the cell operating temperature, H_2 and O_2 were supplied to the anode and cathode at a flow rate of 200 and 1000 mL/min, respectively.

Catalytic activities toward ORR of supported Pt catalysts were examined by electrochemical impedance spectroscopy (EIS) measurements carried out with IM6ex impedance measurement unit (ZAHNER elektrik) at 30 °C. Adsorbed H_2 gas on the Pt(20 wt %)/VC (E-TEK) worked as the counter and the pseudoreference electrode (dynamic hydrogen electrode, DHE). The frequency range investigated was 100 kHz to 10 mHz, and the measurements were made with 10 mV of alternating current (ac) amplitude and 800 mV (vs DHE) of direct current (dc) bias.

3. Results and Discussion

3.1. Surface Morphology and Characterization of the OHNC and the Supported Pt (60 wt %) Catalyst. SEM images of the OHNS and the OHNC are shown in Figure 1. The macropores of both materials reveal a highly

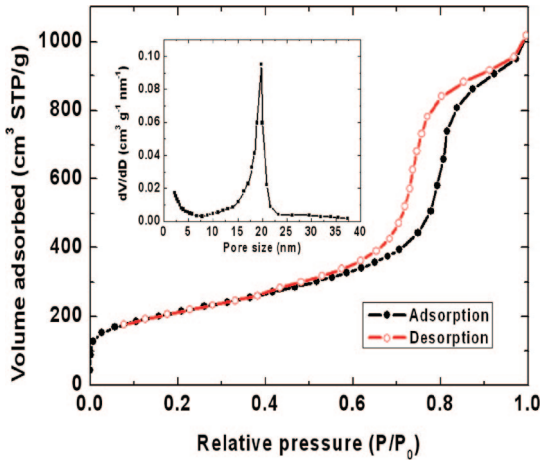

Figure 2. Nitrogen adsorption−desorption isotherm at 77 K and derived PSD for the OHNC.

ordered hexagonal array and were interconnected through small pores (i.e., connecting pores). The SEM image of the OHNS (Figure 1a) shows that macropore sizes (i.e., center-to-center distance between macropores) are approximately 450 ± 10 nm in diameter, the connecting pores are approximately 160 ± 10 nm, and the walls were composed of approximately 23 nm size silica nanoparticles. The SEM image of the OHNC (Figure 1b) shows that the carbon replica was generated from template replication of the OHNS and that the pores of the OHNC are uniform, close-packed, and roughly spherical, resulting in the formation of high surface area multimodal porous carbon framework with highly ordered hierarchical nanostructure. The macropores are approximately 440 ± 10 nm, the connecting pores are approximately 160 ± 10 nm, and the mesopores in the wall are approximately 20 ± 3 nm in the OHNC.

The nitrogen adsorption−desorption isotherm of the OHNC is shown in Figure 2, which is type IV with a H2 hysteresis according to the IUPAC classification, corresponding to framework mesopores. The pore size was estimated from the PSD maximum as approximately 19 nm. The OHNC exhibits a large BET surface area of 962 m^2/g and a total pore volume of 1.93 cm^3/g, mainly attributable to the presence of the mesopores (2 nm < pore size <50 nm) in the framework (mesopore volume: 1.71 cm^3/g), which are much larger than those of the VC (i.e., 230 m^2/g for the BET surface area and 0.22 cm^3/g for the mesopore volume),[73] enabling the OHNC to support high loading of Pt nanoparticles with more uniform dispersion and smaller particle size, as evident from the HRSEM images shown in Figure 3.

The HRSEM image of the commercial carbon black VC-supported Pt (60 wt %) catalyst (Figure 3a) shows that the Pt nanoparticles have particle sizes of approximately 4.2−5.6 nm and that some quantity of Pt nanoparticles have gathered together to form agglomerates with larger particle size. Interestingly, however, Pt nanoparticles are basically deposited separately and homogeneously on the OHNC support with smaller particle size, and they are uniformly distributed on the surface between the mesopores and on the wall of the mesopores, as shown in Figure 3b. The HRTEM image

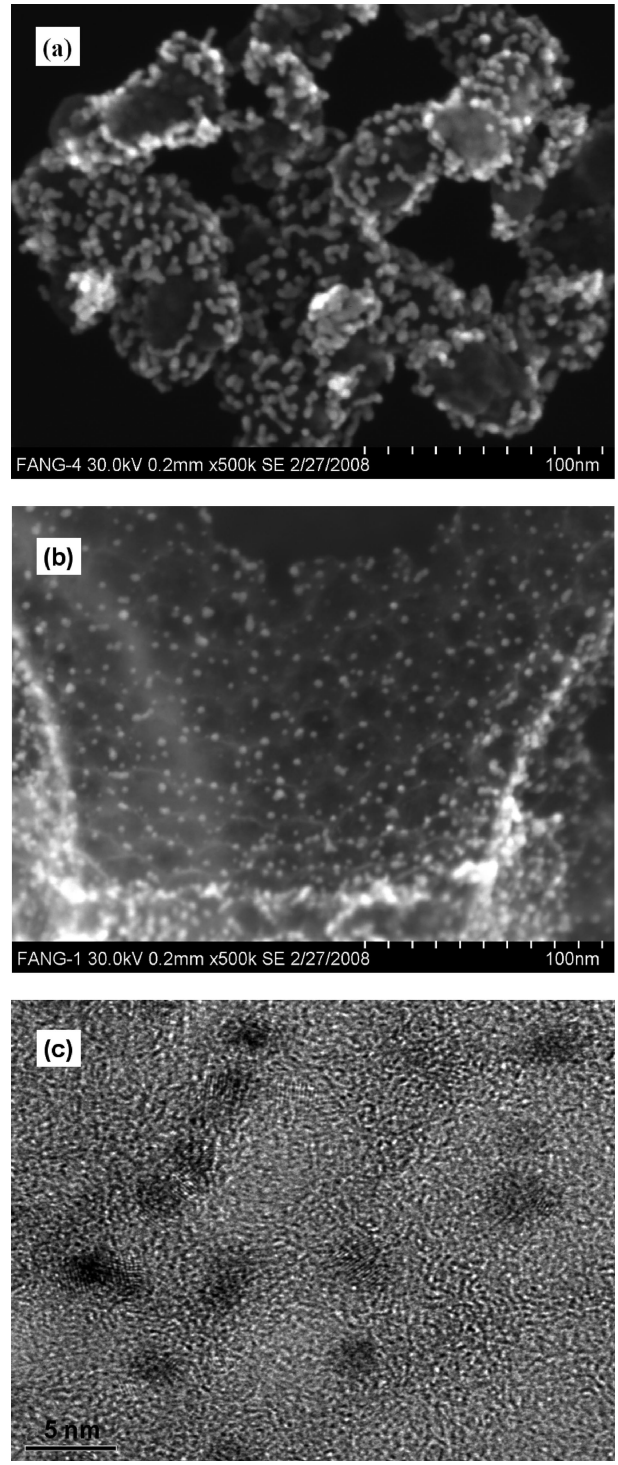

Figure 3. HRSEM images for the Pt (60 wt %)/VC (a), the Pt (60 wt %)/OHNC (b), and HRTEM image for the Pt (60 wt %)/OHNC (c).

(Figure 3c) reveals that most Pt nanoparticles in the Pt (60 wt %)/OHNC have a size of around 3.0 nm.

The XRD patterns of the supported catalysts are shown in Figure 4. Both the supported Pt catalysts exhibit the characteristics of the Pt face-centered cubic structure. The average particle sizes were calculated from the broadening of the Pt (220) reflection as about 5.0 nm for the VC-supported Pt (60 wt %) and 3.3 nm for the OHNC-supported Pt (60 wt %) using a Debye−Scherrer equation. The sizes of the VC or OHNC-supported Pt (60 wt %)

(73) Fang, B.; Kim, M.; Hwang, S.; Yu, J.-S *Carbon* **2008**, *46*, 876–883.

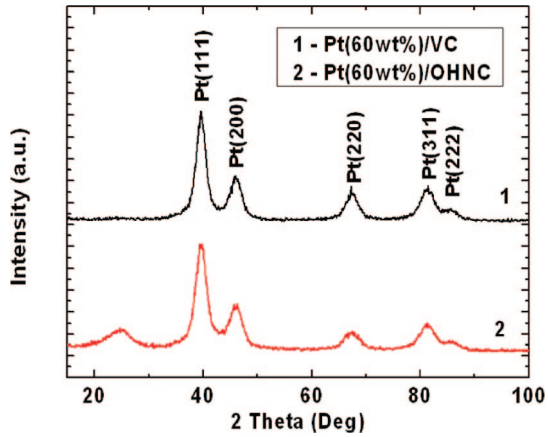

Figure 4. Typical XRD patterns for the VC- or OHNC-supported Pt (60 wt %) catalysts.

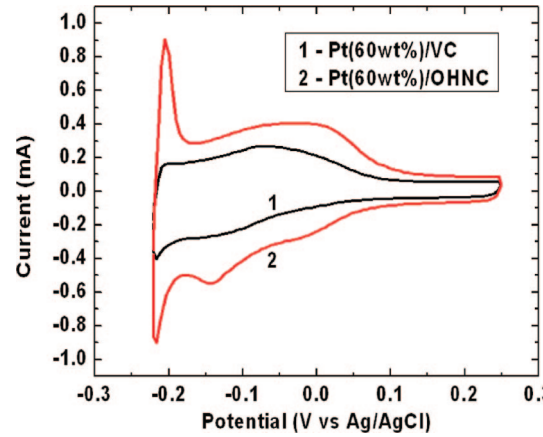

Figure 5. Hydrogen electrosorption voltammetric profiles obtained in 0.5 M H_2SO_4 with a scan rate of 25 mV/s from various carbon-supported Pt (60 wt %) catalyst electrodes; catalyst loading in the working electrode: 63 μg Pt/cm^2.

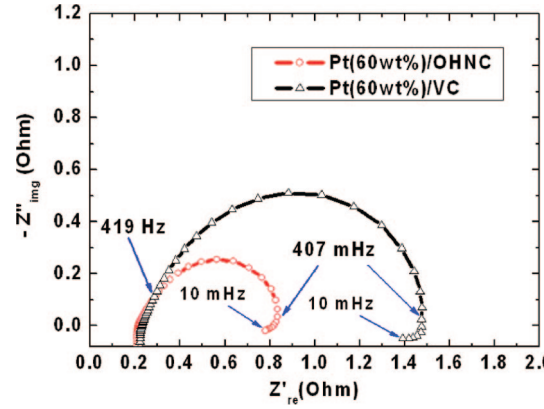

Figure 6. Typical Nyquist plots for the VC- or OHNC-supported Pt (60 wt %) catalyst electrodes; catalyst loading in the test electrodes, 0.2 mg Pt/cm^2; dc bias, 0.8 V (vs DHE); ac amplitude, 10 mV.

nanoparticles are in good agreement with the direct measurements from the HRSEM or HRTEM images shown in Figure 3.

3.2. Electrochemical Active Surface Area of Pt in Supported Pt (60 wt %) Catalyst. Electrochemical active surface areas of Pt in the supported Pt (60 wt %) catalysts were determined from the integrated charge (after subtraction of capacitance contribution) in the hydrogen absorption region of the steady-state cyclic voltammograms in a supporting electrolyte (0.5 M H_2SO_4) and based on a monolayer hydrogen adsorption charge of 0.21 mC/cm^2 on Pt polycrystalline. The current responses in the displayed potential range cannot be completely attributable to the adsorption/desorption of hydrogen because either the VC or the ONHC has very large BET surface area which can accumulate some charge in the electric double layer (EDL). Thus, to calculate the Pt electrochemical active surface area, the contribution of the EDL should be subtracted from the total current response. Compared with the VC, the ONHC has larger BET surface area and hence can accumulate more charge in the EDL, resulting in a lager contribution of the EDL which can be clearly observed in the potential range of 0.15 to 0.25 V where the current response is mainly attributable to the contribution of the EDL. As shown in Figure 5, both the VC- and OHNC-supported Pt (60 wt %) catalysts show the well-known hydrogen adsorption/desorption characteristics for carbon-supported platinum. Electrochemical active surface area was calculated as 68 m^2/g for Pt in the OHNC-supported Pt (60 wt %) nanoparticles catalyst, which is much larger than that (36 m^2/g) for Pt in Pt (60 wt %)/VC, implying better utilization efficiency of Pt/OHNC due to smaller Pt nanoparticles, better dispersion, and more efficient mass transport networks around the Pt nanoparticles supported on the OHNC carbon than on the VC. Larger Pt electrochemical active surface area is expected to provide the OHNC-supported Pt catalyst with higher ORR activity and improved fuel cell performance.

3.3. Catalytic Activities and Polarization Performance of Supported Pt Catalysts. Catalytic activities toward ORR of the VC- or OHNC-supported Pt (60 wt %) cathode catalysts were first evaluated by Nyquist plots shown in Figure 6, from which two high frequency (HF) capacitive loops and one low frequency (LF) inductive loop (i.e., 407 mHz to 10 mHz) were observed. The first small HF loop (>419 Hz) corresponds to the ohmic process within the porous structure of the electrode and membrane[74] while the second HF loop (i.e., 419 Hz to 407 mHz) and the inductive loop (i.e., 407 mHz to 10 mHz) correspond to ORR kinetics[74] and relaxation and diffusion of adsorbed oxygenated intermediate species.[75] It is clear that when the catalyst support changes from the VC to OHNC carbon, the diameter of the second HF loop (i.e., 419 Hz to 407 mHz) decreases dramatically, implying that the ORR charge-transfer resistance is much smaller at the OHNC-supported Pt (60 wt %) cathode catalyst.

Various carbon-supported Pt (60 wt %) catalysts were further evaluated by constant-current polarization performance tests. Figure 7 shows the polarization performance of PEMFC at 60 °C using the VC- or OHNC-supported Pt (60 wt %) cathode catalyst. At low current density, H_2-fueled fuel cell polarization is under electrochemical activation control primarily caused by the sluggish kinetic intrinsic to the ORR at the cathode surface. Smaller polarization voltage loss was observed for the OHNC-supported Pt cathode

(74) Huang, H.; Zhang, W.-K.; Li, M.-C.; Gan, Y.-P.; Chen, J.-H.; Kuang, Y.-F. *J. Colloid Interface Sci.* **2005**, *284*, 593–599.
(75) Antoine, O.; Bultel, Y.; Durand, R. *J. Electroanal. Chem.* **2001**, *499*, 85–94.

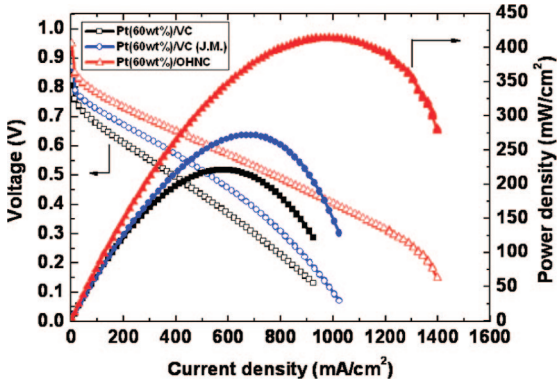

Figure 7. Polarization and power density plots at 60 °C for PEMFCs using the VC- or the OHNC-supported Pt (60 wt %) catalyst cathodes; catalyst loading in the cathodes, 0.2 mg Pt/cm^2.

catalyst than the VC-supported ones, implying that the former catalyst possesses the higher electrocatalytic activity toward ORR, which is primarily attributable to the smaller Pt particle size and better particle distribution in the OHNC-supported Pt cathode catalyst. The maximum power densities are 221 mW/cm^2 for the VC-supported Pt (60 wt %) (homemade), 272 mW/cm^2 for the VC-supported Pt (60 wt %) (Johnson Matthey), and 415 mW/cm^2 for the OHNC-supported one. This corresponds to approximately 53−88% increases in power density of the Pt/OHNC compared to those of the Pt/VC. Much higher power density achieved by the OHNC-supported Pt cathode catalyst than the VC-supported ones is attributable to the unique hierarchical pore structure of the OHNC. First, larger surface area and mesopore volume enable the Pt nanoparticles to deposit more uniformly on the surface of the OHNC with much smaller particle size. Second, the interconnecting ordered larger macropores in combination with mesopores form an open network providing a fast pathway to the active sites (i.e, location of Pt nanopartices), through which the reactant and the products can be readily transported to/away from the active sites, avoiding mass transport limitation. In particular, the mesopore channels with large pore volume open to the macropores are ideal site locations for active Pt nanoparticles, boosting the catalytic reaction and reagent diffusion. Carbon aerogel with similar mesopore size also achieved great ORR performance.[76] In contrast, smaller surface area of the VC with varying pore sizes makes the dispersion of the Pt nanoparticles less uniform with much larger particle sizes, and the randomly distributed pores with broad PSD (from micropores to macropores) and poor pore connectivity in the VC make the mass transport far from being efficient.

3.4. Influence of Metal Loading on Dispersion and Catalytic Performance of the Supported Catalysts. Although catalyst support technology has been proved as a very efficient approach to lower Pt loading in PEMFCs, it still remains a challenge to increase relative Pt wt % in electrode catalysts with the low Pt loading since the increase in relative Pt amount will lower the cost of the supported catalyst due to the reduced amount of catalyst support. As reported by

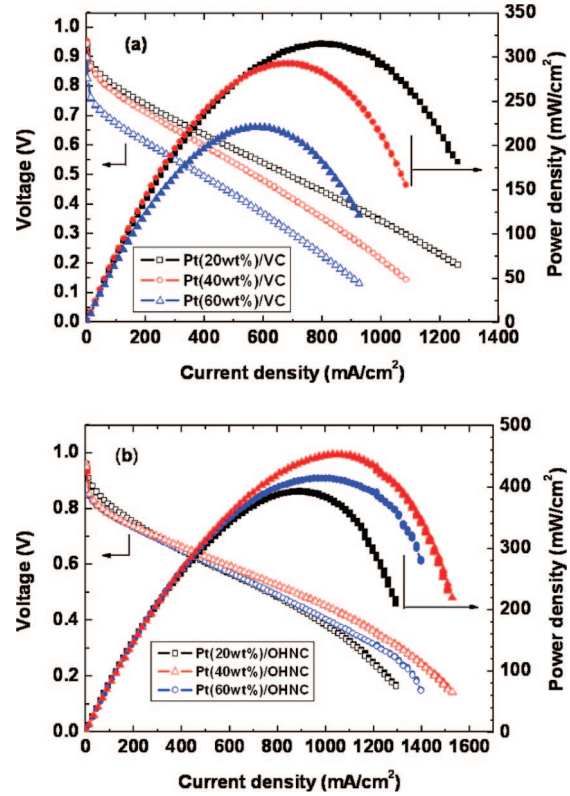

Figure 8. Polarization and power density plots at 60 °C for PEMFCs using the VC- (a) or the OHNC-supported Pt catalyst cathodes (b) with various Pt loadings; catalyst loading in the cathodes, 0.2 mg Pt/cm^2.

Qi et al.,[77] commercial available catalyst Pt (40 wt %)/VC (E-TEK) is inferior to Pt (20 wt %)/VC (E-TEK) in PEMFC performance due to larger Pt particle size of the former (i.e., about twice of the latter) and resulting smaller Pt active surface area. In this study, similar results have been observed for the VC-supported catalysts with various Pt loadings in the range of 20 to 60 wt %, as shown in Figure 8a. The difference in overpotentials is large for the VC-supported catalysts, particularly when Pt loading increased from 40 to 60 wt %, implying that electrocatalytic activity toward ORR decreased considerably when Pt loading increased from 40 to 60 wt % due to the greatly increased particle size of the supported Pt nanoparticles on the VC support and the worse particle distribution. When the Pt loading in the catalyst layer of the VC-supported catalysts changes from 20 wt % to 40 wt %, a decrease of approximately 7% in the maximum power density was observed, while a decrease of approximately 30% was observed when the Pt loading in the VC-supported catalysts changes from 20 wt % to 60 wt %. The main reason for the decrease in the maximum power density is attributable to the increase in the particle size and more uneven dispersion of Pt nanoparticles, as evident from the TEM images shown in Figure S2 in the Supporting Information. When the Pt loading in the VC-supported catalysts changes from 20 wt % to 60 wt %, the size of Pt nanoparticles changes from approximately 3.3 nm to approximately 5.0 nm, resulting in considerable decrease in the Pt active surface area. Furthermore, more agglomeration was observed with the increasing Pt loading, resulting in

(76) Du, H.; Gan, L.; Li, B.; Wu, P.; Qiu, Y.; Kang, F.; Fu, R.; Zeng, Y. *J. Phys. Chem. C* **2007**, *111*, 2040–2043.

(77) Qi, Z.-G.; Kaufman, A. *J. Power Sources* **2003**, *113*, 37–43.

worse dispersion and lower utilization efficiency of the CV-supported Pt nanoparticles. A similar trend in cell polarization performance was observed for the commercially available Pt/VC catalysts from Johnson Matthey, namely, the maximum power density of the VC-supported Pt (60 wt %) (Johnson Matthey) is approximately 272 mW/cm^2, corresponding to a decrease of approximately 17% compared to that (328 mW/cm^2) of the VC-supported Pt (20 wt %) (Johnson Matthey) (the figure not shown). Although the commercial Pt (60 wt %)/VC (Johnson Matthey) has shown much smaller Pt nanoparticles size (i.e., ca. 3.2 nm estimated from the TEM image shown in Figure S3 in the Supporting Information) and better dispersion than the one prepared by the microwave-assisted ethylene glycol method in this study due to the more superior catalyst preparation method employed in Johnson Matthey, it seems impossible for the VC-supported high metal loading (i.e., 60 wt %) Pt catalyst to have better polarization performance than the VC-supported low metal loading (i.e., 20 wt %) Pt catalyst at low Pt loading (i.e., 0.2 mg Pt/cm^2) in the cathode. Interestingly, however, the OHNC-supported Pt catalysts have demonstrated completely different images; namely, with the increasing Pt loading in the catalyst layer from 20 wt % to 40 wt %, the maximum power density delivered by the supported Pt catalyst increases by approximately 15.2%, and when the Pt loading in the catalyst layer increases from 20 wt % to 60 wt %, a slight increase by approximately 5.6% in the maximum power density is still observed. The reasons for the enhanced power density can be explained as follows. Although Pt loading in the catalyst layer of the OHNC-supported catalysts increases from 20 wt % to 60 wt %, the particle size of the Pt nanoparticles supported on the OHNC increases slightly from 2.6 to 3.3 nm as shown in Figure S4 of the Supporting Information and in Figure 4. In addition, the Pt nanoparticles are still highly homogenously dispersed on the OHNC even with a loading as high as 60 wt %. The slight increase in particle size and uniform dispersion of the Pt nanoparticles supported on the OHNC is solely contributable to the large surface area and mesopore volume, and the fantastic hierarchical nanostructure of the OHNC. The slight increase in the particle size of the supported Pt nanoparticles may result in some limited decrease in the Pt active surface area and in catalytic activity. On the other hand, however, with the same Pt loading of 0.2 mg/cm^2 in the cathode, one-third of the catalyst amount required by Pt (20 wt %)/OHNC was used in the case of Pt (60 wt %)/OHNC, resulting in a much thinner diffusion layer due to less carbon required, less void volume in the electrode, and accordingly much smaller resistance from the mass diffusion. In addition, a thinner catalyst layer with less void volume is also favorable for the formation of the triple-phase boundary, resulting in enhanced utilization of Pt nanoparticles. Both of the above-mentioned factors are expected to improve fuel cell performance greatly despite some negative effect such as increased particle size for relative high metal loading in the OHNC.

Compared with the commercial carbon black VC, the OHNC seems to be much better candidate to support Pt nanoparticle effectively especially with high relative Pt loading (i.e., 40 or 60 wt %), which is highly desired to lower the cost of the supported catalyst due to the reduced amount of catalyst support (i.e., carbon). The higher metal loading is also preferred in supported catalysts for PEMFCs, leading to significant decrease in stack weight and size, which are greatly favorable for fuel efficiency and internal system design in fuel cell power-driven mobile system application.

4. Conclusions

In this study, OHNC has been fabricated through a simple nanocasting approach and explored for the first time as a cathode catalyst support in PEMFC. As a result of its fantastic characteristics, such as ordered hierarchical nanostructure, large surface area, and mesopore volume, the OHNC can support high loading of Pt nanoparticles with uniform dispersion and small particle size. Compared to the VC-supported Pt (60 wt %) cathode catalyst, the OHNC-supported Pt (60 wt %) has demonstrated greatly enhanced catalytic activity toward ORR and considerably improved PEMFC performance, suggesting that the OHNC is a very promising highly efficient cathode catalyst support in PEMFC. Furthermore, the OHNC-supported high metal loading Pt catalysts (i.e., 40 or 60 wt %) outperform the OHNC-supported low metal loading Pt catalyst (i.e., 20 wt %) even at a low catalyst loading of 0.2 mg Pt/cm^2, which represents a significant breakthrough in fuel cell technology because the fabricating cost of the supported noble metal catalyst and the system weight can be reduced greatly due to the considerable decrease in the required amount of catalyst support while high fuel cell performance can be still achieved through the usage of unique catalyst support OHNC.

Through careful control of the precursor of OHNS and/or OHNC, the size of mesopores and macropores can be tailored readily. In addition, ordered carbon with hierarchical nanostructure of macropores in combination with mesopores and micropores can be easily fabricated, which can expand the applications of the OHNCs to other fields such as adsorbent, hydrogen storage, and Li ion battery electrode material. Further development of the OHNCs with various hierarchical nanostructure and other potential applications are under investigation.

Acknowledgment. The authors would like to thank the WCU Program and BK21 Program for financial support and the Korean Basic Science Institute at Jeonju, Chuncheon, and Daejeon for SEM, TEM, and XRD measurements.

Supporting Information Available: Diagram of electrical conductivity for various carbon materials and TEM images for carbon black VC- or OHNC-supported Pt catalysts with various metal loadings (i.e., 20, 40, and 60 wt %; PDF). This material is available free of charge via the Internet at http://pubs.acs.org.

CM801467Y